This is a repository copy of *Assessing the integrity of steel structural components with stress raisers using the Theory of Critical Distances*.

White Rose Research Online URL for this paper:
http://eprints.whiterose.ac.uk/103333/

Version: Accepted Version

Article:

Li, W., Susmel, L. orcid.org/0000-0001-7753-9176, Askes, H. et al. (2 more authors) (2016) Assessing the integrity of steel structural components with stress raisers using the Theory of Critical Distances. Engineering Failure Analysis, 70. pp. 73-89. ISSN 1350-6307

https://doi.org/10.1016/j.engfailanal.2016.07.007

Article available under the terms of the CC-BY-NC-ND licence
(https://creativecommons.org/licenses/by-nc-nd/4.0/)

Reuse
This article is distributed under the terms of the Creative Commons Attribution-NonCommercial-NoDerivs (CC BY-NC-ND) licence. This licence only allows you to download this work and share it with others as long as you credit the authors, but you can’t change the article in any way or use it commercially. More information and the full terms of the licence here: https://creativecommons.org/licenses/

Takedown
If you consider content in White Rose Research Online to be in breach of UK law, please notify us by emailing eprints@whiterose.ac.uk including the URL of the record and the reason for the withdrawal request.

eprints@whiterose.ac.uk
https://eprints.whiterose.ac.uk/

Accepted Manuscript

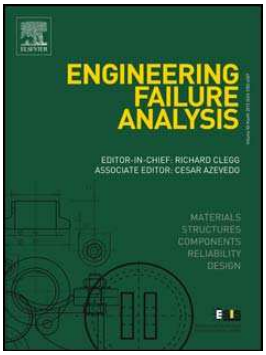

Assessing the integrity of steel structural components with stress raisers using the Theory of Critical Distances

Wenchao Li, Luca Susmel, Harm Askes, Fangfang Liao, Tianhua Zhou

PII: S1350-6307(16)30261-8
DOI: doi: 10.1016/j.engfailanal.2016.07.007
Reference: EFA 2944

To appear in:

Received date: 1 May 2016
Revised date: 6 July 2016
Accepted date: 26 July 2016

Please cite this article as: Li Wenchao, Susmel Luca, Askes Harm, Liao Fangfang, Zhou Tianhua, Assessing the integrity of steel structural components with stress raisers using the Theory of Critical Distances, (2016), doi: 10.1016/j.engfailanal.2016.07.007

This is a PDF file of an unedited manuscript that has been accepted for publication. As a service to our customers we are providing this early version of the manuscript. The manuscript will undergo copyediting, typesetting, and review of the resulting proof before it is published in its final form. Please note that during the production process errors may be discovered which could affect the content, and all legal disclaimers that apply to the journal pertain.

ACCEPTED MANUSCRIPT

Assessing the integrity of steel structural components with stress raisers using the Theory of Critical Distances

Wenchao Li [a,b,*], Luca Susmel [b], Harm Askes [b], Fangfang Liao [a], Tianhua Zhou [a]

[a] School of Civil Engineering, Chang'an University, Xi'an 710061, China

[b] Department of Civil and Structural Engineering, The University of Sheffield, Mappin Street, Sheffield S1 3JD, United Kingdom

***Corresponding Author:** Mr. **Wenchao Li**
School of Civil Engineering
Chang'an University, Xi'an, Shaanxi Province, 710061, China
Telephone: +86 13709147632
E-mail: wenchaoli@chd.edu.cn

Abstract: This paper assesses and evaluates the detrimental effect of standard and complex geometrical features on the static strength of samples made of Q460 steel. The experimental results generated by testing four types of notched specimens were analyzed using the Theory of Critical Distances (TCD). The considered configurations included uniaxial tension tests on standard notched round bars and double-side U-notched flat plate specimens. In particular, our attention was focused on the fracture behavior of two specimens containing complex geometrical features subjected to pure-shear and tensile-shear local stress states. The common feature of these two notched specimens was that cracks were seen to initiate, within the material, away from the stress raisers, even though obvious stress concentrations existed at notch tip. The performed validation exercise confirms the accuracy and reliability of the linear-elastic TCD in estimating the fracture initiation position and static strength of standard notched round bars and double-side U-notched flat plate specimens. In the meantime, the linear-elastic method proposed in this paper can also be used as an effective approach to assess the fracture behavior of metallic components having complex geometry.

Key words: notches; Theory of Critical Distances; static failure; fracture; structural steel

ACCEPTED MANUSCRIPT

1.Introduction

Many engineering investigations have demonstrated that failure of engineering components takes place in the vicinity of notches, cracks and complex geometrical features. Further, micro defects due to manufacturing usually tend to concentrate themselves in these regions with a weakening effect on the overall strength of the components. In parallel, stress concentration phenomena and the resulting local multiaxial stress states accelerate the crack initiation process. In this context, it is key to provide structural engineers with design methods suitable for evaluating the detrimental effect of notches on the overall strength of engineering components.

The Theory of Critical Distances (TCD) [1] is a group of failure criteria which make use of the local linear-elastic stress fields in the vicinity of the assumed crack initiation locations to estimate the fatigue and fracture strength of notched components. The key feature of the TCD is that the relevant stress fields are post-processed by using a material dependent length scale parameter. The fundamental ideas on which the TCD is based can be dated back to the pioneering work carried out by Neuber [2] and Peterson [3] in the twentieth century. Neuber [2] proposed to calculate an effective stress to estimate the high-cycle fatigue strength of notched components by averaging the linear-elastic stress over a line emanating from the assumed crack initiation point. A few years later, Peterson [3] simplified the above approach by suggesting that the effective stress can directly be calculated by simply using the stress at a given distance from the notch apex. Subsequently, studying the notch effect on the static strength of fiber composites, Whitney and Nuismer [4] established the link between the critical distance and Linear Elastic Fracture Mechanics (LEFM), where the material's characteristic length can directly be determined through the LEFM fracture toughness and the material's ultimate tensile strength. These methods were then reformulated by Taylor [1, 5-6] to make them suitable for addressing different structural integrity problems.

In recent years, a tremendous effort has been made by the scientific community to extend the use of the TCD to other ambits of the structural integrity discipline. In more detail, this theory was demonstrated to be successful in estimating the static strength of notched brittle and quasi-brittle material (such as PMMA, cement, rocks) [7-10] as well as of notched ductile metallic material

ACCEPTED MANUSCRIPT

subjected to uniaxial [11,12] and multiaxial static loading [13,14]. More recently, Ameri et al. [15] have proven that the TCD, applied in conjunction with the Von Mises equivalent stress, is successful in predicting the static strength of welded joints. Further, the TCD was seen to be highly accurate also in estimating the fracture strength of notched metallic materials under dynamic loading by introducing a strain rate term in its formulation [16].

In contrast to other material failure theories which are based on elasto-plastic analysis (e.g. the phenomenological ductile fracture theories for crack-free bodies [17]), the most appealing feature of the TCD is its simplicity: various types of non-linearities can be accommodated into a framework that is entirely linear-elastic. Furthermore, when using the TCD to design real components, the static assessment can be performed by introducing only two additional material parameters, which can be determined easily using conventional standard testing equipment.

A review of the available literature suggests that the overall reliability and accuracy of the TCD was verified mainly by using standard stress raisers, whose crack initiation locations were unambiguously known *a priori* and whose detrimental effect could be assessed directly by using a bi-dimensional model. On the contrary, real engineering components often contain complex geometrical features, where the location of the crack initiation is not always obvious, especially in the presence of complex multiaxial loading. It was demonstrated in a recent research conducted by Louks et al.[18] that the TCD used in conjunction with Modified Wöhler Curve Method (MWCM) is capable of giving a high-level accuracy in estimating the fatigue strength of a number of components containing complex/3D geometrical notches subjected to a complex multiaxial fatigue load history, where, however, the common feature of these investigated specimens was that the crack was observed to initiate at the stress raiser apices.

It is well-known that, for some real notched engineering components, cracks do not initiate at the stress raiser tips, but in the interior area of the component, i.e., away from the highly stressed regions. In other words, the cracking behavior of such notched components is not governed by the mechanical behavior of the material in the vicinity of the stress raisers being assessed.

In this complex scenario, this paper aims to use the linear-elastic TCD to estimate fracture initiation locations and static strength of notched samples made of high-strength structural steel

ACCEPTED MANUSCRIPT

Q460 subjected to uniaxial and local multiaxial loading. Initially, the reliability and accuracy of the TCD were checked against a large number of experimental results generated by testing standard notched round bar and double-side U-notched flat plate specimens under uniaxial tensile loading. Subsequently, attention was focused on the performance of the TCD in assessing the fracture behavior of two specimens containing complex geometrical features subjected to local pure-shear and tensile-shear loading, where the common feature of these two specimens was that the crack was observed to initiate away from the stress raiser tips.

2. Fundamentals of the Theory of Critical Distances

Real engineering components often contain transitional geometrical features at connection regions. Such transitional geometrical features usually can be understood as notches which result in stress concentration phenomena.

Consider a notched engineering component with an arbitrary geometry subjected to a complex system of forces - Fig.1(a). Stresses usually tend to concentrate in the local area at the notch root. Thus, the overall strength of the component is controlled and can be directly estimated by assessing the local stress field in the vicinity of the notch tip.

The Theory of Critical Distances (TCD) [1] postulates that the static strength of notched/cracked engineering materials can be predicted by directly post-processing the local linear-elastic stress field in the vicinity of the notch root or crack tip via a characteristic material length parameter. The basic assumption of this method is that the static failure of a notched component will occur when the effective stress σ_{eff}, determined from the linear-elastic stress field in the vicinity of the stress raiser apex being assessed, exceeds the material inherent strength σ_0. In the determination of the effective stress σ_{eff}, several strategies were proposed in the literature, which include the Point Method (PM), Line Method (LM) and the Area Method (AM). The principles for each of these methods are illustrated in Fig.1.

The PM (see Fig.1(b)) is the simplest formalization of the TCD. According to Peterson's idea [3], the PM postulates that the static strength of a notched component can be estimated by using the stress state at a given distance from the apex of the stress raiser under investigation. The static

ACCEPTED MANUSCRIPT

failure of the component being assessed is assumed to occur when the effective stress σ_{eff} at a distance equal to $L/2$ from the notch tip on the straight line experiencing maximum stress gradient equals the material inherent strength σ_0:

$$\sigma_{\mathrm{eff}} = \sigma\left(\theta = 0, \mathrm{r} = \mathrm{L}/2\right) = \sigma_0 \qquad \text{Point Method} \qquad (1)$$

The static strength of a notched component can also be predicted via an effective stress determined by averaging the linear-elastic stress over a line (see Fig.1(c)) or a semicircular area centered at the apex of the notch (see Fig.1(d)), i.e. the LM and AM, respectively:

$$\sigma_{\mathrm{eff}} = \frac{1}{2\mathrm{L}} \int_0^{2\mathrm{L}} \sigma\left(\theta = 0, \mathrm{r}\right) = \sigma_0 \qquad \text{Line Method} \qquad (2)$$

$$\sigma_{\mathrm{eff}} = \frac{2}{\pi \mathrm{L}^2} \int_{-\pi/2}^{\pi/2} \int_0^{\mathrm{L}} \sigma(\theta, \mathrm{r}) \mathrm{r} \mathrm{d}\mathrm{r} \mathrm{d}\theta = \sigma_0 \qquad \text{Area Method} \qquad (3)$$

In the above definitions, σ is the equivalent linear-elastic stress at the notch tip, which can be calculated according to one of the classic hypotheses (such as Von Mises, Tresca, maximum principal stress criterion, etc.), whereas L and σ_0 are the so-called material critical distance and the inherent strength, respectively. Both L and σ_0 are material constants. The most accurate way to determine these two material properties is to test samples containing, at least, two different geometrical features [1,11,14]. Fig. 2 schematically depicts the specific steps for determining L and σ_0, where the two stress-distance curves are plotted, in the incipient failure condition, in terms of the adopted equivalent stress obtained by testing a sharp and blunt notch, respectively. According to the PM, the coordinates of the point at which these two curves intersect each other directly gives the values of both L and σ_0. In what follows, we will use the TCD in conjunction with Von Mises' and Tresca's effective stress.

Furthermore, attention should be paid as defining the straight line used to determine the effective stress σ_{eff} (see Fig.1). This line is usually referred to as the focus path. Generally, for notched specimens with standard stress raisers, since the crack initiation location is in known *a priori* unambiguously, the focus path can be assumed to emanate from the crack initiation point and is parallel to the direction experiencing the maximum stress gradient. However, it was reported in a recent investigation [18] that, for notched components characterized by complex 3D geometries, the

ACCEPTED MANUSCRIPT

position of the potential crack initiation location would change depending on the degree of multiaxiality and non-proportionality of the loading path being applied. In this scenario, when using the TCD, static strength has to be estimated by choosing several potential focus paths to find the one which experiences the maximum extent of damage.

3. Calibration of the TCD material parameters for steel Q460

3.1 Material

The material considered in this study is Chinese low-alloy high-strength structural steel Q460 (with nominal yield strength equal to 460 MPa) [19]. Table 1 gives the nominal chemical composition of the investigated steel. In order to obtain the conventional mechanical properties of this material, three smooth round bar specimens (see Fig.3(a)) with geometry designed according to ASTM E8/E8M-11 [20] were tested under uniaxial tensile loading. The tested specimens were machined from a block of 36 mm thick hot rolled steel plate with the longitudinal axis along the rolling direction. Fig.4 shows the engineering stress-strain curves obtained from the smooth round bar tensile tests, where the obtained mechanical properties for the investigated steel are as follows: Young's modulus, E=222758 MPa; average yield stress, σ_y=430.7 MPa; ultimate tensile stress σ_{UTS}=570.8 MPa; and elongation at fracture equal to 57%. All the notched specimens considered in the following sections were machined from the same parent steel plate in order to guarantee the investigated material properties to be consistent.

3.2 Notched round bar specimens subjected to uniaxial tensile loading

In order to estimate the values of L and σ_0, 9 standard notched round bar specimens with three different values of the notch radii were machined and tested under uniaxial tensile loading. The geometry of the notched round bar specimen (see Fig.3(a)) is the same as that of the smooth round bar specimen described above, with a circumferential notch being introduced in the central area of the specimen. Three values of the notch radius, i.e. 6.25 mm, 3.125 mm and 1.5 mm, were considered. The initial diameter of the gross and net cross section were equal to 12.5 mm and 6.25 mm, respectively. Before testing, the notched round bar specimens were labeled as BN-1-9 (three specimens were machined for each notch radius).

ACCEPTED MANUSCRIPT

The uniaxial tension tests involving the notched round bar specimens were carried out by using an MTS universal testing machine with a 200 kN load cell. During testing, the nominal uniaxial elongation in the notch region was measured by using an extensometer having gauge length equal to 20 mm. The generated experimental results, including the dimension measured before/after testing, the ultimate tension loads and the adopted loading rate, are summarized in Table 2.

Fig.5(a) shows the profile of some load-displacement curves for each type of notched round bar specimen. The load-capacity and ductility of the tested samples were observed to be strongly sensitive to the sharpness of the notch: the yield and ultimate nominal tensile load of the notched round bar specimens were seen to increase with the decrease of the notch radius. The displacement measured at the ultimate load and the reduced diameter of the net section after failure (see Table 2) were seen to decrease with the decrease of the notch tip radius.

In addition, Fig.6(a) shows the fracture profile for each type of notched round bar specimen. A typical cup-and-cone rough fracture surface surrounded by 45° shear lips was observed at the notch root for each specimen. Moderate necking was also observed at the fracture surface, which indicates that final breakage was characterized by a ductile mode.

After conducting the experiments, the linear-elastic stress fields in the vicinity of the notch root of the notched round bar specimens were post-processed by using FE software ABAQUS/Standard. The mechanical behavior of the steel being tested was assumed to obey a linear-elastic constitutive law. Axisymmetric two-dimensional FE models (see Fig.7) were solved to determine the relevant linear-elastic stress fields. In order to obtain accurate results, the mesh density in the vicinity of the notch tip was gradually increased until convergence occurred, this process resulting in elements having, in the process zone, a size of the order of 0.05 mm.

As an example, Fig.7 shows both the Von Mises and Tresca stress contours, obtained in the incipient failure condition, at the root of the notched round bar specimen having a notch radius equal to 3.125 mm. The incipient failure condition here is defined as the maximum load recorded during testing. As shown in Fig.7, the position of the hot spot for the notched round bar specimen is univocal, directly corresponding to the notch tip. Thus, the focus path was defined as a straight line emanating from the notch tip, with such a line being also fully in accordance with the observed crack

ACCEPTED MANUSCRIPT

path orientation (see Fig.6(a)).

According to the experimental technique sketched in Fig.2, the chart of Fig.8 shows the stress-distance curves obtained on the corresponding focus paths of the notched round bar specimens in terms of Von Mises and Tresca equivalent stress, respectively. Each curve is obtained by using the average results generated from the three round bar specimens in the same sample types. Due to the usual errors associated with experiments, these curves are seen not to pass through the same point. As to the determination of the TCD material properties, the standard procedure suggested in the literature (e.g. Ref.[1,11,14]) to determine both L and σ_0 is based on the use of two stress-distance curves characterized by different stress gradients. In other words, it is generally accepted that using two sets of results generated by testing bluntly and sharply notched specimens, respectively, allows both the critical distance and the material inherent strength to be determined accurately. Therefore, according to this idea, the values of L and σ_0 adopted in the present study were determined by using the results generated from the samples containing the bluntest and sharpest notch, i.e. the bars having notch radius equal to 6.25 mm and 1.5 mm, respectively. For the investigated Q460 steel, this process resulted in the following TCD material parameters: L=1.026 mm and σ_0=649.6 MPa when the Von Mises equivalent stress was adopted for the assessment; and L=1.058 mm and σ_0=684.2 MPa when the Tresca equivalent stress was adopted for the assessment. This result clearly indicates that the values of the TCD material parameters depend on the adopted definition for the equivalent stress.

4. Validation of the TCD by experimental data

After determining the values of L and σ_0, the TCD can be used to estimate the fracture initiation location and static strength of the notched component being assessed. The potential crack initiation point can be located by identifying the position of the hot spot on the component, and the overall static strength of the component can be estimated by comparing the magnitude of the effective stress σ_{eff}, determined in the vicinity of the notch tip, with the material inherent strength σ_0.

In order to assess the reliability of the TCD, in what follows the accuracy of this theory will be checked against a number of experimental results generated by testing both standard and complex

ACCEPTED MANUSCRIPT

geometrical features under uniaxial tensile and local multiaxial loading.

4.1 Double-side U-notched flat plate specimen subjected to uniaxial loading

The first geometry which was investigated to check the accuracy of the TCD is a flat plate with transversal U-notches on both sides (see Fig.3(b)). These specimens were machined from a rectangular sheet having length × width × thickness equal to 150 mm × 50 mm × 5 mm. In order to introduce the wanted stress concentration phenomena at the critical area, symmetric circumferential notches with three different notch radius values, i.e. 10 mm, 3 mm and 1 mm, were machined on both sides of the middle section of the sheet. The cross-sectional thickness at notch root and clamping section of the sample were 2 mm and 5 mm, respectively.

Under uniaxial tensile loading, the specific geometry of the double-notched flat plate resulted in a plane strain condition at the center of the notch due to the confinement of the deformation along the groove length direction. Hence, such a geometry was used to investigate the fracture behavior of the material being assessed under plane strain condition [21]. For each notch radius, two specimens were machined and tested under uniaxial loading. Before testing, the double-notched flat plate specimens were labelled as GP-1-6. During testing, the uniaxial elongation of the notch region was measured by using an extensometer having gauge length equal to 20 mm. The measured cross-sectional thickness at the notch root and the loading rate applied to the double-notched flat plate specimens are summarized in Table 2.

The load-displacement curves and the fracture modes for the double-notched flat plate specimens are presented in Fig.5(b) and 6(d), respectively. Similar to the mechanical behavior of the notched round bar specimens discussed in the previous section, the load-capacity and ductility of the tested double-notched flat plate samples were seen to be governed by the sharpness of the notch, even though the net cross-sectional areas were identical. During the loading process, cracks were seen to initiate at the central area of the notch region (see Fig.9(b)), that is, the region experiencing the largest strain confinement. The crack subsequently propagated along the direction perpendicular to the axis of the specimen. Further, it should be noted that, similar to what observed by Susmel and Taylor in Refs [13, 14], the maximum load in the load-displacement curve of the

ACCEPTED MANUSCRIPT

double-notched flat plate specimens was seen to correspond to the presence of a visible crack on the specimen surface. Such phenomena were also observed for both the pure-shear and tensile-shear notched specimen described in the following sections (see the following section 4.2 and 4.3). This suggests that, for the investigated samples, the maximum load recorded during the test could be used to define the incipient failure condition.

The linear-elastic stress fields at the notch root of the double-notched flat plate specimen were post-processed by using a 3D FE model as shown in Fig.9(a). Due to the obvious symmetry in three planes, only 1/8 of the specimen was modelled. The minimum element size adopted at the notch root region of the sample was refined down to 0.1 mm in order to estimate the required stress field accurately.

As an example, Fig.9(c) shows the Von Mises stress contour at the notch tip of the flat plate specimen with notch radius equals to 3 mm (the corresponding Tresca stress contour at the notch tip of the sample is similar to this result). Due to the simplicity of the geometry, as expected, the maximum stress point, i.e. the hot-spot, was, at the notch tip, at the midsection of the sample, that is, at the specimen section experiencing the largest degree of stress triaxiality. Such a hot spot position fully agrees with the observed crack initiation location during testing (see Fig.9(b)). Accordingly, the focus path was assumed to emanate from the notch tip being parallel to the specimen's thickness direction (see Fig.9(a)).

For each double-notched flat plate specimen, the charts of Fig.9(d-e) show the stress-distance curves obtained, in the incipient failure condition, on the corresponding focus paths in terms of Von Mises and Tresca equivalent stress, respectively. Each curve is calculated as the average from the results obtained for the same sample type. In order to evaluate the accuracy of the PM and LM, the effective stress σ_{eff} calculated through Eq.(1) and (2) is compared with the material inherent strength σ_0. Table 3 and Table 4 summarize the accuracy of the PM and LM, used in terms of Von Mises and Tresca equivalent stress, for all the tested flat plate samples, where the results predicted by the TCD for all the notched round bar specimens are also reported. The error was calculated according to the following equation:

ACCEPTED MANUSCRIPT

$$\text{Error} = \frac{\sigma_{\text{eff}} - \sigma_0}{\sigma_0} \times 100\% \tag{4}$$

In Eq.(4), the prediction is conservative when the value of the error is positive; whereas the prediction is non-conservative when the value of the error is negative.

The results reported in Table 3-4 make it evident that the TCD used in conjunction with both Von Mises and Tresca equivalent stress is highly accurate in predicting the static fracture strength of notched Q460 under nominal uniaxial tension loading. The estimates of the PM and LM for both the notched round bar and double-notched flat plate specimens fall within an error interval of ±20%. Further, it should be noted in Table 4 that, when the Tresca stress is adopted as the equivalent stress, the LM could not be used to estimate the strength of the specimen GP-3, 4, 6, since the value of 2*L* has exceeded the measured thickness at the notch of the sample (see Table 2).

Table 3-4 also summarize the level of scattering charactering the results obtained for each type of specimen being investigated. As it can be observed from Table 3-4, with the exception of specimens GP-5 and GP-6 (i.e. the double-notched flat plate specimen having notch radius equals to 1 mm), the level of scattering obtained by applying both the PM and LM for the same type of specimen is quite limited. It is the authors' opinion that the large scattering level associated with specimens GP-5 and GP-6 is mainly due to the existing difference in terms measured thickness at notch root of the samples (see Table 2), this returning different values for the experimental ultimate loads (see Table 2). However, as it can be observed from Table 3-4, the predictions made by applying the PM and LM still fall within an error interval of ±20%. This error is considered to be acceptable, since, in general, it is not possible to distinguish between an error of ±20% and an error of 0% due to those problems which are usually encountered during testing as well as during the numerical analyses [6].

4.2 Complex geometrical notched specimen subjected to local pure shear loading

In order to further check the accuracy of the TCD in predicting the strength of notched steel Q460 under local pure-shear stress state, a flat plate specimen characterized by the complex geometry shown in Fig.3(c) was tested under uniaxial tension loading. In Refs.[22-24], the geometry

ACCEPTED MANUSCRIPT

of this type of specimen was shown to result in a nearly pure-shear stress state at the butterfly-shaped gauge section, with the crack initiation location being controlled by changing the shape and opening angle of the upper and lower notches. For example, cracks can be forced to initiate at the upper/lower notch tip of the gauge section by using a crack-like notch with a small opening angle. On the contrary, cracks can be initiated at the interior region (i.e., away from the notch surface) by using a blunt notch with a larger opening angle. In order to force the crack to initiate at the gauge area, the adopted cross-sectional thickness of the gauge and the clamping section were different, where the thickness of the former and latter ones were 2 mm and 4 mm, respectively.

In the present paper, the notch manufactured at the upper and lower edge of the gauge section was a round blunt notch having an opening angle equals to 90° and notch radius equals to 2 mm. Two specimens were machined and labelled as FP-1,2. To apply the tensile load, pinned bolts were inserted in the holes at both the upper and lower clamping sections. The obtained ultimate load and loading displacement rate for the pure-shear flat plate specimen are reported in Table 2.

Fig.5(c) shows the load-displacement curve of the pure-shear flat plate specimen, where a yielding plateau with a long plastic displacement phase is observed before breakage takes place. It should be pointed out also that, during the loading phase, the crack was seen to initiate at the interior region (see the red cross in Fig.10(d)) rather than at the surface in the vicinity of the upper and lower notch. This phenomenon is very interesting, since it indicates that the global fracture behavior of notched components is not necessarily governed by local stress concentration phenomena. In other words, the complex geometry being investigated makes the flat plate specimen behave in a manner similar to that of a plain specimen even though stress raisers exist at the critical region of the gauge section.

Figs.10(b-c) show the Von Mises stress field, plotted in the incipient failure condition, at the gauge section of the pure-shear flat plate specimen. This stress-field was determined by using a finite element model (Fig.10(a)) with a minimum mesh size of 0.1 mm at the gauge area. As it can be observed from Fig.10(b), due to the complex geometry of the gauge area, several stress concentration points combined with local multiaxial stress states appear at the upper and lower

ACCEPTED MANUSCRIPT

notch root simultaneously. Accordingly, the positions of the hot spot and the corresponding focus path cannot be defined unambiguously.

In order to use the TCD to evaluate the failure condition of the pure-shear specimen, here, we use an alternative method to determine the fracture initiation position and the focus path of the sample. As described in section 2, the basic assumption of the PM is to ignore the stress at the crack/notch tip, and use the stress information at a given distance away from the notch tip to estimate the failure strength of the component. According to this idea, we can draw a curvilinear path at a distance of $L/2$ away from the surface and use the stress information obtained on this path to determine the failure condition of the specimen being assessed. In such circumstances, the potential crack initiation point can be assumed to occur at the point experiencing the largest stress on this critical path, whereas the focus path can be defined as a straight line passing through such a maximum stress point and perpendicular to the surface.

According to the idea discussed above, Fig.10(c) shows such a critical path located, at the lower notch region in the mid-plane of the gauge section, at a distance equal to $L/2$ away from the notch surface. The relevant stress distribution obtained on this path is presented in Fig.10(e). Due to the anti-symmetry of the geometry, the stress distribution obtained from the corresponding path at the upper notch is mirrored by that shown in Fig.10(e). As it can be observed in Fig.10(e), the largest Von Mises stress magnitude is obtained at material point B with a stress value equal to 811 MPa. Such a stress level is higher than the value of σ_0, which indicates failure has occurred at this region.

It should also be recalled here that, according to the cracking behavior displayed by the pure-shear flat plate specimens, the crack was seen to initiate in a region away from the notch area (see Fig.10(d)). This result suggests that, when using the TCD, one should not only focus his attention on the local stress information at the notch, since the stress value at a material point away from the notch region may be higher than that on any points on the arc path we used for determining the fracture initiation location. Under such circumstances, the crack would initiate internally rather than in the notch tip region.

According to this idea, the stress information in the internal area of the gauge section was

ACCEPTED MANUSCRIPT

subsequently investigated. The stress distribution shown in Fig.10(c) suggests that the material point experiencing the largest stress magnitude in the internal area of the gauge section corresponds to point F. The stress value obtained at this point, which is equal to 814 MPa, is slightly higher than the value obtained at point B, suggesting that the crack could also initiate at this point. This observation is in full agreement with the experimental result shown in Fig.10(d).

Further, in order to clearly compare the prediction results obtained from the two stress strategies (i.e. Von Mises and Tresca stress) investigated in the present study, the performance of the Tresca stress criterion, used along with the TCD, was investigated subsequently. Fig.11 shows the Tresca stress field obtained, under the same conditions we used to determine the Von Mises stress, at the gauge section of the pure-shear specimen. As it can be observed in Fig.11,The distribution of the Tresca stress at gauge area of the sample is similar to that of the Von Mises stress (Fig.10(c)), where local high stresses were observed to appear at both the notch and internal regions simultaneously. In order to estimate the fracture initiation location, similar to the procedure we used for the Von Mises stress, the Tresca stress fields at both the notch and interior regions were investigated, respectively. It is shown that the points experiencing the maximum stress magnitude at the critical path and internal material region are also corresponding to the material point B and point F, respectively. However, the difference in terms of stress magnitude between the internal point F (938 MPa) and material point B (821 MPa) is more evident, which further proves that the crack was initiated at the interior material region. These results, combined with the results obtained from the Von Mises stress criterion, confirm that the use of the linear-elastic TCD allowed the potential fracture initiation location to be estimated quite accurately for this sample. This proves that such a design method is capable of modelling the fracture behavior of notched components under pure-shear stress state, this holding true independently of the complexity of the geometry being assessed.

Since the crack was initiated at the interior material region, the fracture behavior of the pure-shear notched specimen is similar to the one displayed by a plain (i.e., un-notched) specimen. Such a fracture condition falls outside the application range of the TCD, since this theory is designed to specifically assess stress raisers rather than un-notched components [1]. In this

ACCEPTED MANUSCRIPT

scenario, according to classic continuum mechanics, the ultimate tensile stress σ_{UTS}, which is usually adopted as the strength limit for the un-notched material, should be used to estimate the static strength of the pure-shear specimen. In such circumstances, the expression for the error in Eq.(4) should be modified as:

$$\text{Error} = \frac{\sigma_{\max} - \sigma_{\text{UTS}}}{\sigma_{\text{UTS}}} \times 100\% \tag{5}$$

where σ_{max} is the maximum value of the Von Mises' or Tresca's equivalent stress obtained at the internal gauge area of the sample. According to the results shown in Fig.10(c) and Fig.11, σ_{eff}=814 MPa when the Von Mises equivalent stress was adopted for the analysis, and σ_{eff}=938 MPa when the Tresca equivalent stress was adopted for the analysis. The results calculated according to Eq.(5) shows that, for the investigated Von Mises and Tresca stress criteria, the estimated errors obtained using the ultimate tensile stress σ_{UTS} as the strength limit are about 43% and 64%, respectively. It is the authors' opinion that such conservative results are to be ascribed to the confinement effect of the material around the crack initiation location, which delays the actual crack initiation process. Further, it is also believed that the magnitude of the load at which the crack initiated was lower than the maximum force recorded during testing. The fact that the initiation of a crack at one material point does not correspond to the complete breakage of the component being tested should explain why a conservative result was obtained by using the standard continuum mechanics approach along with the ultimate tensile stress.

4.3 Complex geometrical notched specimen subjected to local tensile shear loading

The notched specimen considered in the present section is a flat plate involving an oblique gauge area located at the center of the specimen. In Refs.[22,25] the geometry of this sample (see Fig.3(d)) is shown to be capable of producing a mixed tensile-shear stress state at the gauge area when the specimen is tested under uniaxial tensile loading. The axis of the gauge region is designed to be at 20 degrees to the loading axis of the specimen. In order to force the crack to initiate in the gauge area, the gauge section of the tensile-shear specimen was designed to be thinner than that of the clamping section, where the thickness of the former and the latter ones were

ACCEPTED MANUSCRIPT

2 mm and 4 mm, respectively.

Contrary to the geometry we used in the early research [25], no notch was employed at the gauge section of the tensile-shear specimen in the present study, thus this region behaves in a manner more like a plain specimen. However, blunt round notches, having a notch radius equals to 3 mm and opening angle equal to 80 degrees, were introduced as a transitional feature between the gauge and clamping sections (see Fig.3(d)). Such a complex geometry makes the crack initiation location of the specimen ambiguous, since the crack could initiate either at the notch root or in the gauge area.

Two tensile-shear flat plate specimens were machined and tested under uniaxial tensile loading by using an MTS universal testing machine, where the specimens were labelled as GP-3,4 before testing. The relevant experimental results generated for the tensile-shear flat plate specimens are summarized in Table 2.

The load-displacement curves and the fracture profile of the tensile-shear specimen are presented in Fig.5(d) and 6(c), respectively. Similar to the fracture behavior of the pure-shear specimen, the crack on the tensile-shear specimen was observed to initiate at the center of the oblique gauge section (see the red cross position in Fig.12(d)) rather than at the notch root in the transitional region. The crack subsequently propagated forming a fracture surface being at about 60° to the loading direction. Such a fracture initiation location suggests that the notch in the transitional region between the gauge and clamping section had no detrimental effect on the overall strength of the sample. In addition, necking was also observed at the fracture surface, which indicates that the cracking behavior of the tensile-shear specimen was characterized by a ductile mode.

Fig.12(b-c) shows the Von Mises stress field, plotted in the incipient failure condition, obtained at the gauge area of the tensile-shear specimen by using the 3D FE model shown in Fig.12(a) (where the minimum mesh size in gauge area is 0.1 mm). Such a stress distribution confirms that stress concentration phenomena exist at the surface area of the transitional notch roots. Further, due to the complexity of the geometry, high stress values were also observed to localize at both the sides and the central region of the gauge section of the sample.

ACCEPTED MANUSCRIPT

In order to determine the fracture initiation location of the tensile-shear specimen, similar to the procedure we used to predict the failure condition for the pure-shear specimen, the stress field located at the notch root area of the sample was investigated first. Fig.12(c) shows the critical path located at the mid-plane of the gauge section of the tensile-shear specimen with a distance of $L/2$ from the surface area of the notch root. The relevant Von Mises stress-distance curve extracted on this path is presented in Fig.12(e). It is interesting to observe (Fig.12(e)) that the stress value extracted in front of the maximum stress point at the stress raiser, i.e. material point B, is lower than the material inherent strength σ_0. Such a result explains the reason why the crack was not initiated at the notch root, since the material at this region was far from reaching its strength limit. In addition, the material point experiencing the largest stress magnitude was seen to be point D on the critical path, which is located at the side of the gauge section. In the incipient failure condition, the stress value at this point (761.1 MPa) was larger than the material inherent strength (σ_0=649.6 MPa), suggesting that the failure process started in this region.

Subsequently, our attention was focused on the stress information located at the interior region of the tensile-shear specimen. The Von Mises stress contour in Fig.12(c) shows that the material point experiencing the largest stress magnitude in the interior area appears at the central point of the gauge zone (i.e. point F), with a stress value equal to 732.6 MPa. This stress level is slightly lower than that obtained at material point D (i.e., 761.1 MPa). This result slightly deviates from the observed experimental result.

Since the results obtained by using the Von Mises equivalent stress were not that accurate, we tried to re-analyse the generated results using the Tresca's equivalent stress. Fig.13 shows the Tresca stress field obtained, under the same conditions we used to determine the Von Mises stress, at the gauge section of the tensile-shear specimen. The difference in terms of stress magnitude between central point F (817.5 MPa) and material point D (762.7MPa) is more evident, which suggests that the crack was initiated at the central region. Further, one can also find that the straight line which connects the central point F to point D is right in accordance with the direction of the maximum shear stress. Such a direction is observed to coincide with the propagation direction of the fracture surface as well.

ACCEPTED MANUSCRIPT

According to the results described above (and compared with the results obtained from the Tresca stress criterion), the use of Von Mises equivalent stress seems slightly less successful in estimating the fracture initiation location of the tensile-shear specimen. However, according to the results in Fig.12(c), the difference in terms of stress magnitude between the central point F and material point D obtained from the Von Mises stress criterion is not obvious, which is within an internal of 5%. Such a result suggests that there was an evident competition between the notch effect and the intrinsic strength of the tested material during the test for this specimen. Further, it is demonstrated in the previous sections that the two equivalent stresses strategies resulted in the same level of accuracy in estimating the static strength of the notched Q460 steel components. In this scenario, our recommendation for predicting the cracking behavior of the tensile-shear specimen is to consider the results calculated by using both Von Mises' and Tresca's equivalent stress.

To conclude, since in this specimen type the crack was seen to initiate in the interior region, the static strength of the tensile-shear specimen could successfully be estimated by using the Von Mises or Tresca stress value determined at point F (see Fig.12(c) and Fig.13), i.e. 732.6 MPa or 817.5 MPa, respectively. According to Eq.(5), for the adopted Von Mises and Tresca equivalent stress, the errors calculated using the ultimate tensile stress as the strength limit are equal to 28.3% and 43.2%, respectively, which are not only low, but also conservative.

5. Discussion

The aim of the present paper is to investigate the reliability and accuracy of the linear-elastic TCD in assessing and evaluating the detrimental effects of notches on the overall behavior of notched samples made of steel Q460. According to the results obtained in the present study, the considered notches have an obvious influence on the overall behavior of the standard samples subjected to uniaxial tensile loading. The overall static strength, ductility and the fracture initiation location of the notched round bar and double-side U-notched flat plate specimens being assessed were observed to be strongly controlled by the mechanical behavior of the material in the vicinity of the notch root area. Under such circumstances, the linear-elastic TCD, applied in terms of both Von

ACCEPTED MANUSCRIPT

Mises and Tresca equivalent stress, was seen to be successful in estimating the static strength of the these samples by directly post-processing the linear-elastic local stress fields acting on the material in the vicinity of the notch tip, resulting in estimates falling within an error interval of ±20%.

On the contrary, according to the cracking behaviors observed from the pure-shear and tensile-shear flat plate specimens, we can conclude that, for some notched specimens containing complex geometrical features, cracks may initiate in a region away from the stress raisers. In this sense, the overall fracture mode of such notched specimens is transferred from a "local-controlled" mode to a "global-controlled" mode due to the considered complex geometry and material properties. Under such circumstances, according to the design procedure we propose in the present study, the fracture initiation location of such a notched component can be estimated by directly finding the maximum stress point in the material region having a distance of $L/2$ away from the surface of the notch root. Accordingly, the static strength of the component can be estimated by comparing the stress value obtained at this maximum stress point with the corresponding material strength limit, i.e. the σ_0 or σ_{UTS}.

Further, it should be noted that, since the TCD method is a local approach which shares the basic assumption of Linear Elastic Fracture Mechanics and is based on the local mechanical information in front of the stress raiser, this method is not valid for estimating the failure condition of the "global-controlled" notched specimen, which actually behave in a manner like a plain specimen. Under such circumstances, the overall static strength of the notched component being assessed is estimated by using the theory which is suitable for estimating the fracture of plain specimen, e.g. the ultimate tensile stress used in the present study.

In addition, it is worth mentioning that if σ_0 (rather than σ_{UTS}) was used as the material strength limit to estimate the static strength of the pure-shear and tensile-shear specimens, the prediction error for these two notched geometries would be significantly reduced (taking the results obtained from Von Mises stress criterion as examples, the prediction error for the pure-shear specimen will be reduced from 43% down to 25% and that for tensile-shear specimen will be reduced from 28% to 13%). In the meantime, according to the stress fields results for these two specimens in Fig.10(b) and Fig.12(b), we can find that obvious stress gradients were also present around the internal

ACCEPTED MANUSCRIPT

maximum stress region. Such a result seems to indicate that these internal material regions can also be treated as stress raisers, even though these regions are away from the notch. The results described above seem to suggest to use σ_0 rather than σ_{UTS} to assess these complex notched specimens, since σ_0 can be considered as a local material strength index capable of taking into account the stress gradient effect when plastic deformation are ignored [11]. However, attention must be paid when using this approach since no previous work in this field suggests that the internal material region can be regarded as a stress raiser and addressed by using a local failure theory. However, we think that such a usage can be considered as an open question which needs more and further works to be answered properly.

Finally, it is also interesting to discuss why the linear-elastic TCD method can work for the linear-elastic conditions. According to the TCD's *modus operandi*, we can see that, via length *L*, the magnitude of the effective stress used to evaluate the extent of damage is reduced compared to that of the linear-elastic stress field close to the apex of the geometrical feature being assessed. Accordingly, in the incipient failure condition, this mimics the smoothing effect of plasticity on the local stress fields. This simple argument may explain why the linear-elastic TCD is successful in estimating the static strength of ductile notched materials.

6. Conclusions

This paper summarizes an attempt to use the linear-elastic TCD to estimate the fracture initiation location and static strength of notched samples made of Q460 high-strength steel subjected to uniaxial and multiaxial stress states. The reliability and accuracy of the PM and LM, used in conjunction with Von Mises and Tresca equivalent stress, were checked against the experimental results generated by testing four types of notched specimens. The main conclusions can be summarized as follows:

(1) The linear-elastic TCD can successfully be used to estimate the static strength of notched ductile Q460 steel subjected to nominal uniaxial loading. The estimates of both the PM and LM for the standard notched round bar and double-side U-notched flat plate specimens are seen to fall within an error interval of ±20% when the methods are formalized in terms of Von Mises or

ACCEPTED MANUSCRIPT

Tresca equivalent stress.

(2) For the pure-shear and tensile-shear flat plate specimen being assessed in the present paper, which contained complex geometrical features and were subjected to local pure-shear and multiaxial stress states, the cracks were seen to initiate at the interior area of the specimen rather than at the surface area of the stress raiser. Under such circumstances, the strength of these specimens was assessed according to classic continuum mechanics.

Acknowledgements

The work presented herein is supported by the Natural Science Foundation of China (Grant No. 51408055), the Fundamental Research Funds for the Central Universities (Grant No. 310828151070) and the Science Foundation for Post Doctorate Research of Shaanxi Province. The first author is sponsored by the China Scholarship Council (Grant No. 201406560006).

Reference

[1] D. Taylor, The theory of critical distances: a new perspective in fracture mechanics. Elsevier, Oxford, UK, 2007.

[2] H. Neuber, Theory of notch stresses: principles for exact calculation of strength with reference to structural form and material, 2nd ed., Springer Verlag, Berlin, 1958.

[3] R.E. Peterson, Notch sensitivity, in: G. Sines, J.L. Waisman (Eds.), Metal fatigue, McGraw Hill, New York, 1959, pp. 293-306.

[4] J.M. Whitney, R.J. Nuismer, Stress fracture criteria for laminated composites containing stress concentrations, J. Compos. Mater. 8 (1974) 253-265.

[5] D. Taylor, Geometrical effects in fatigue: a unifying theoretical model, Int. J. Fatigue 21 (1999) 413-420.

[6] D. Taylor, The theory of critical distances, Eng. Fract. Mech. 75 (2008) 1696-1705.

[7] D. Taylor, Predicting the fracture strength of ceramic materials using the theory of critical distances, Eng. Fract. Mech. 71 (2004) 2407-2416.

[8] L. Susmel, D. Taylor, The theory of critical distances to predict static strength of notched brittle components subjected to mixed-mode loading, Eng. Fract. Mech. 75 (2008) 534-550.

[9] S. Cicero, V. Madrazo, I.A. Carrascal, Analysis of notch effect in PMMA using the Theory of Critical Distances, Eng. Fract. Mech. 86 (2012) 56-72.

[10] S. Cicero, T. García, J. Castro, V. Madrazo, D. Andrés, Analysis of notch effect on the fracture behaviour of granite and limestone: An approach from the Theory of Critical Distances, Eng. Geol. 177 (2014) 1–9.

ACCEPTED MANUSCRIPT

[11] L. Susmel, D. Taylor, On the use of the Theory of Critical Distances to predict static failures in ductile metallic materials containing different geometrical features, Eng. Fract. Mech. 75 (2008) 4410-4421.

[12] V. Madrazo, S. Cicero, I.A. Carrascal, On the Point Method and the Line Method notch effect predictions in Al7075-T651, Eng. Fract. Mech. 79 (2012) 363-379.

[13] L. Susmel, D. Taylor, The Theory of Critical Distances to estimate the static strength of notched samples of Al6082 loaded in combined tension and torsion. Part I: Material cracking behaviour, Eng. Fract. Mech. 77 (2010) 452-469.

[14] L. Susmel, D. Taylor, The Theory of Critical Distances to estimate the static strength of notched samples of Al6082 loaded in combined tension and torsion. Part II: Multiaxial static assessment, Eng. Fract. Mech. 77 (2010) 470-478.

[15] A.A.H. Ameri, J.B. Davison, L. Susmel, On the use of linear-elastic local stresses to design load-carrying fillet-welded steel joints against static loading, Eng. Fract. Mech. 136 (2015) 38-57.

[16] T. Yin, A. Tyas, O. Plekhov, A. Terekhina, L. Susmel, A novel reformulation of the Theory of Critical Distances to design notched metals against dynamic loading, Mater. Des. 69 (2015) 197-212.

[17] Y. Bai, T. Wierzbicki, A comparative study of three groups of ductile fracture loci in the 3D space, Eng. Fract. Mech. 135 (2015) 147-167.

[18] R. Louks, B. Gerin, J. Draper, H. Askes, L. Susmel, On the multiaxial fatigue assessment of complex three-dimensional stress concentrators, Int. J. Fatigue. 63 (2014) 12-24.

[19] GB/T 1591-2008. High strength low alloy structural steels. Beijing: China Standard Press, 2008.(in Chinese).

[20] ASTM E8/E8M-11, Standard test methods for tension testing of metallic materials, ASTM International, West Conshohocken, PA, 2011. doi:10.1520/E0008_E0008M-11

[21] Y. Bai, X. Teng, T. Wierzbicki, On the application of stress triaxiality formula for plane strain fracture testing, J. Eng. Mater. Technol. 131 (2009) 021002.

[22] Y. Bao, T. Wierzbicki, On fracture locus in the equivalent strain and stress triaxiality space, Int. J. Mech. Sci. 46 (2004) 81-98.

[23] Q. Sun, D. Zan, J. Chen, H. Pan, Analysis of edge crack behavior of steel sheet in multi-pass cold rolling based on a shear modified GTN damage model, Theor. Appl. Fract. Mech. 80 (2015) 259-266.

[24] G. Gruben, E. Fagerholt, O.S. Hopperstad, T. Børvik, Fracture characteristics of a cold-rolled dual-phase steel, Eur. J. Mech. A/Solids. 30 (2011) 204-218.

[25] L. Susmel, D. Taylor, Non-propagating cracks and high-cycle fatigue failures in sharply notched specimens under in-phase Mode I and II loading, Eng. Fail. Anal. 14 (2007) 861-876.

ACCEPTED MANUSCRIPT

List of captions:

Table 1. Chemical composition of Q460 steel (in weight%)

Table 2. Experimental results of the notched specimens tested in this paper

Table 3. The accuracy of the PM and LM, used in conjunction with Von Mises stress, in predicting the static strength of notched round bar and double-notched flat plate specimens tested under uniaxial loading conditions

Table 4. The accuracy of the PM and LM, used in conjunction with Tresca stress, in predicting the static strength of notched round bar and double-notched flat plate specimens tested under uniaxial loading conditions

Figure 1. local coordinate system located at the notch tip of the notched component subjected to a complex system of forces (a); the working principle of the Point Method (b); Line Method (c); and the Area Method (d).

Figure 2. Determination of the material critical distance L and inherent strength σ_0 through two linear-elastic stress-distance curves generated by testing two notched specimens with different notch sharpness under nominal uniaxial loading.

Figure 3. Geometries of the tested specimens: smooth and notched round bars (a); double-side U-notched flat plate specimens (b); pure-shear flat plate specimen (c); and tensile-shear flat plate specimen (d). (dimensions in millimeters).

Figure 4. Engineering stress-strain curves of Q460 steel

Figure 5. Load-displacement curves of the tested specimens: notched round bar specimens (a); double-side U-notched flat plate specimens (b); pure-shear flat plate specimen (c); tensile-shear flat plate specimen (d).

Figure 6. Fracture profiles of the tested specimens: notched round bar specimens (a); pure-shear flat plate specimen (b); tensile-shear flat plate specimen (c); double-side U-notched flat plate specimens (d).

Figure 7. Von Mises and Tresca stress field located at the notch root of notched round bar specimen (notch radius=3.125 mm).

Figure 8. Stress-distance curves obtained on the corresponding focus paths of the notched round bar specimens: Von Mises stress (a); Tresca stress (b).

Figure 9. Finite element model and the focus path of double-side U-notched flat plate specimen (a); observed fracture initiation location of the sample in the test (b); Von Mises stress fields obtained at the notch root area (c); stress-distance curves obtained on the focus paths of the double-side U-notched flat plate specimens: Von Mises stress (d); Tresca stress (e).

Figure 10. Finite element model developed for the pure-shear flat plate specimen (a); Von Mises stress fields located at the gauge section (b); the critical path located at the lower notch region of the specimen (c); the observed experimental fracture initiation location (d); Von Mises stress-distance curve obtained on the critical path (e).

ACCEPTED MANUSCRIPT

Figure 11. Tresca stress fields located at the gauge section of the pure-shear specimen and the relevant stress-distance curve obtained on the critical path.

Figure 12. Finite element model developed for the tensile-shear flat plate specimen (a); Von Mises stress fields located at the gauge section (b); the critical path located at the notch region of the tensile-shear specimen (c); the observed experimental fracture initiation location (d); stress-distance curve obtained on the critical path (e).

Figure 13. Tresca stress fields located at the gauge section of the tensile-shear specimen and the relevant stress-distance curve obtained on the critical path.

ACCEPTED MANUSCRIPT

ACCEPTED MANUSCRIPT

Figures

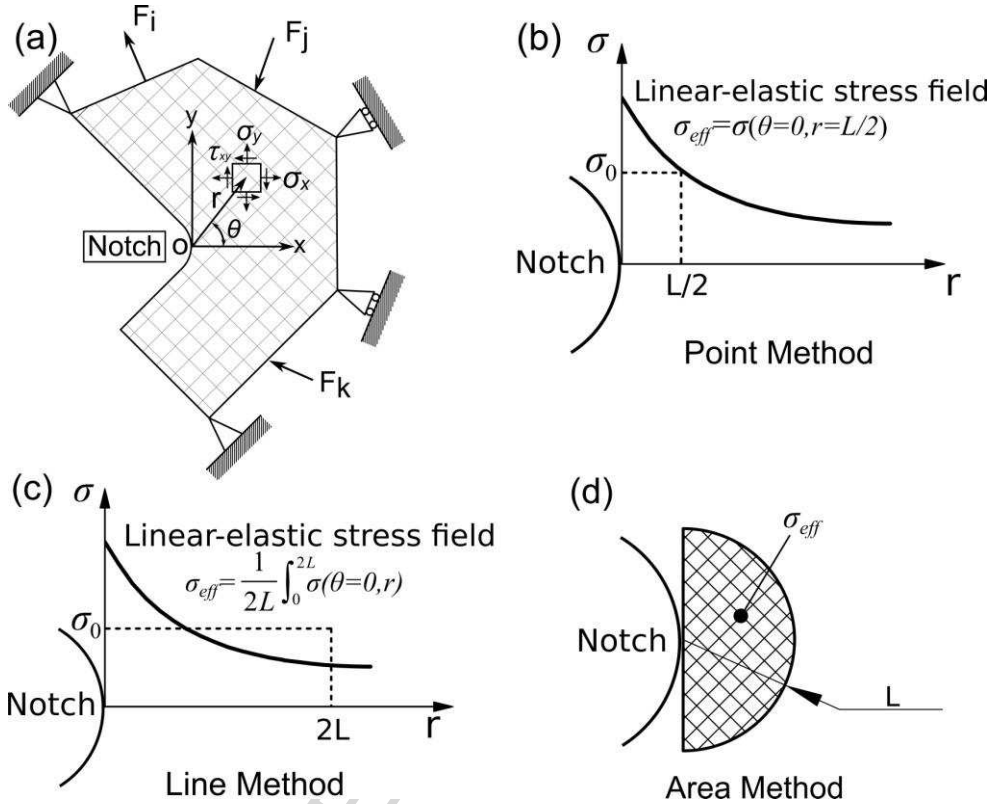

Figure 1. local coordinate system located at the notch tip of the notched component subjected to a complex system of forces (a); the working principle of the Point Method (b); Line Method (c); and the Area Method (d).

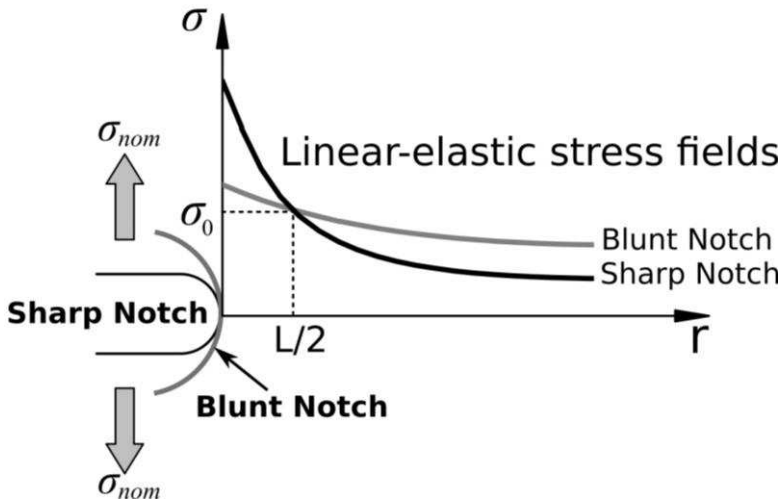

Figure 2. Determination of the material critical distance *L* and inherent strength σ_0 through two linear-elastic stress-distance curves generated by testing two notched specimens with different notch sharpness under nominal uniaxial loading.

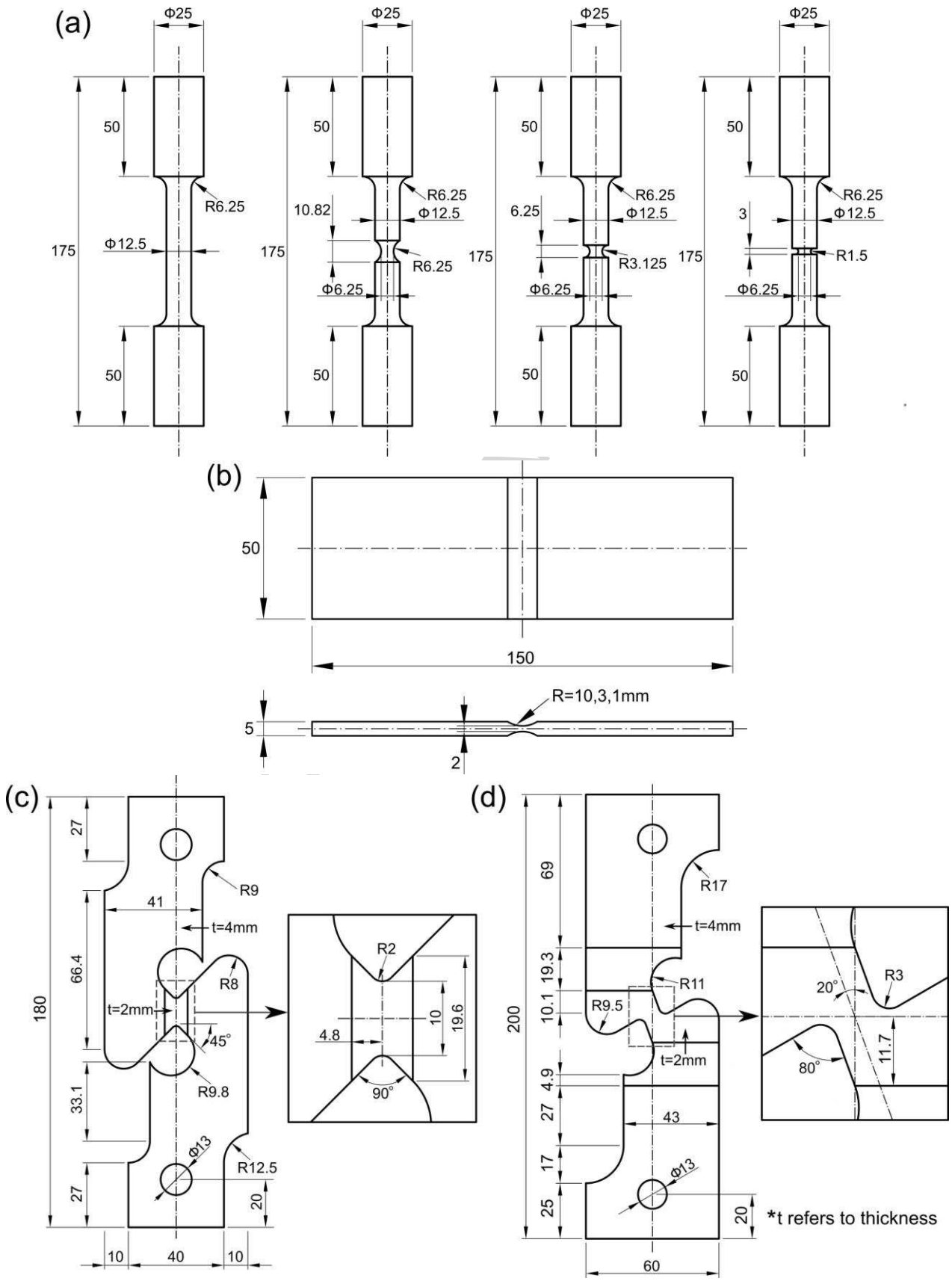

Figure 3. Geometries of the tested specimens: smooth and notched round bars (a); double-side U-notched flat plate specimens (b); pure-shear flat plate specimen (c); and tensile-shear flat plate specimen (d). (dimensions in millimeters).

ACCEPTED MANUSCRIPT

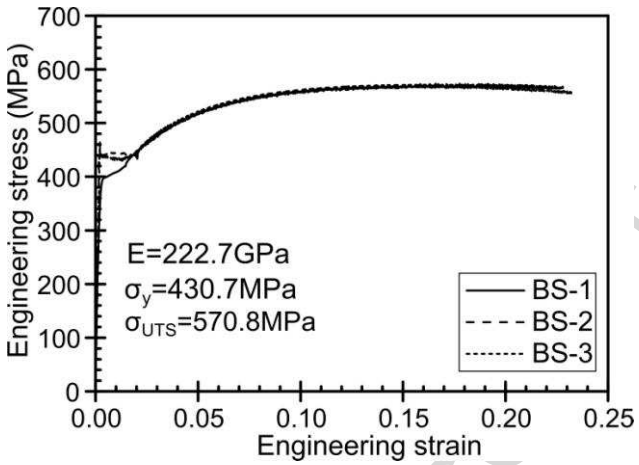

Figure 4. Engineering stress-strain curves of Q460 steel

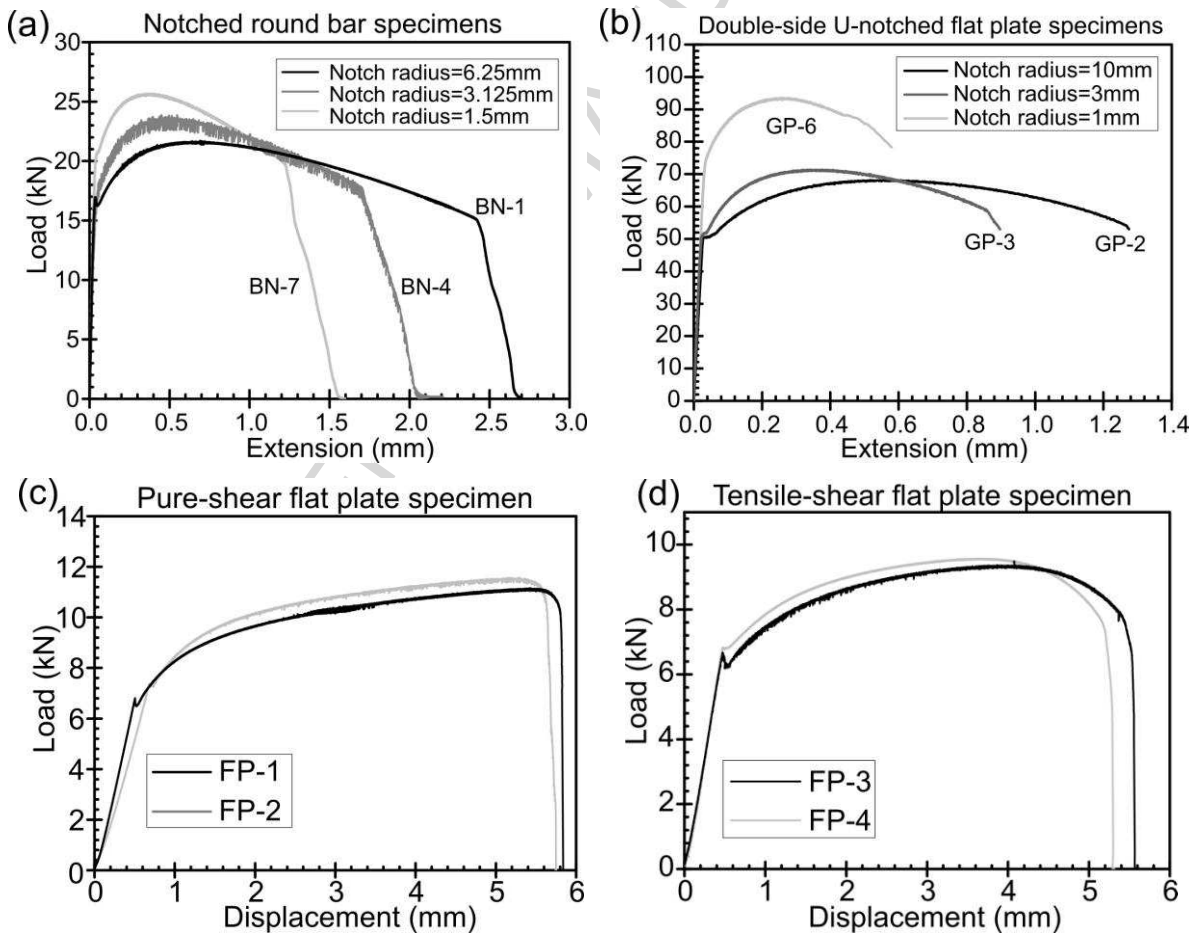

Figure 5. Load-displacement curves of the tested specimens: notched round bar specimens (a); double-side U-notched flat plate specimens (b); pure-shear flat plate specimen (c); tensile-shear flat plate specimen (d).

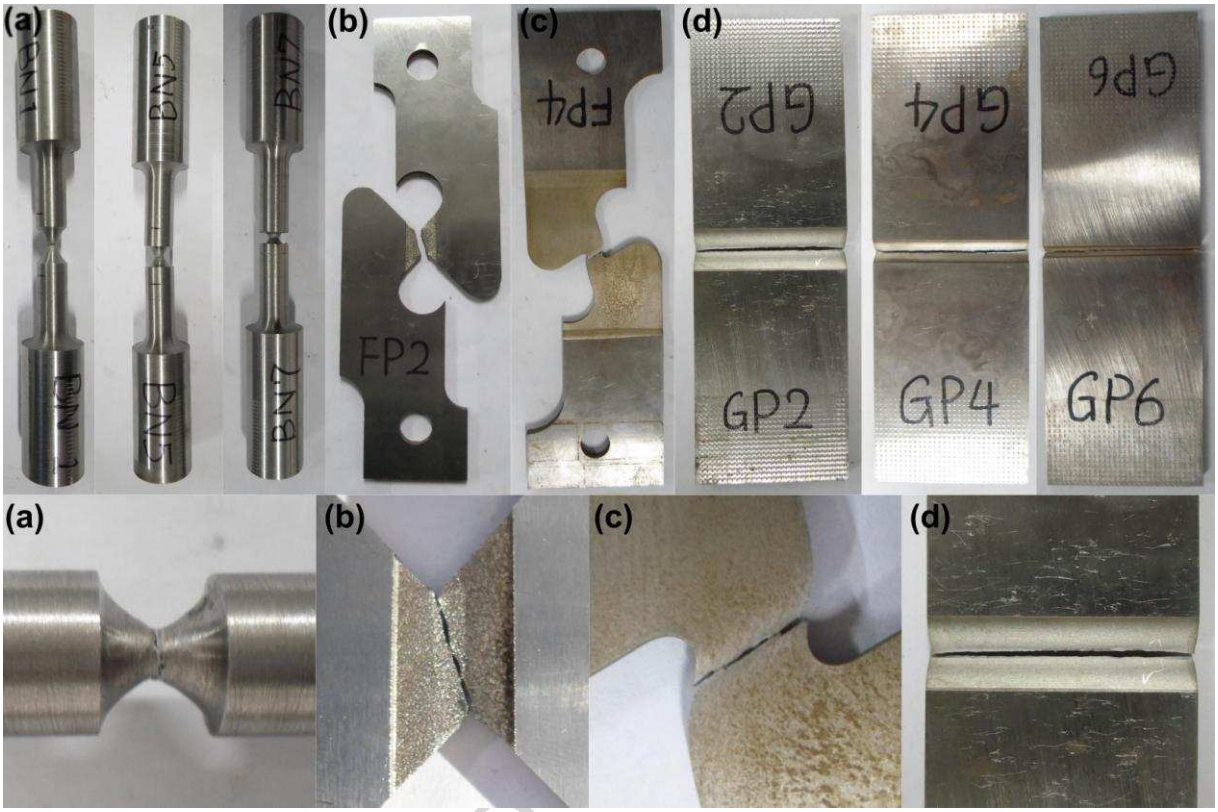

Figure 6. Fracture profiles of the tested specimens: notched round bar specimens (a); pure-shear flat plate specimen (b); tensile-shear flat plate specimen (c); double-side U-notched flat plate specimens (d).

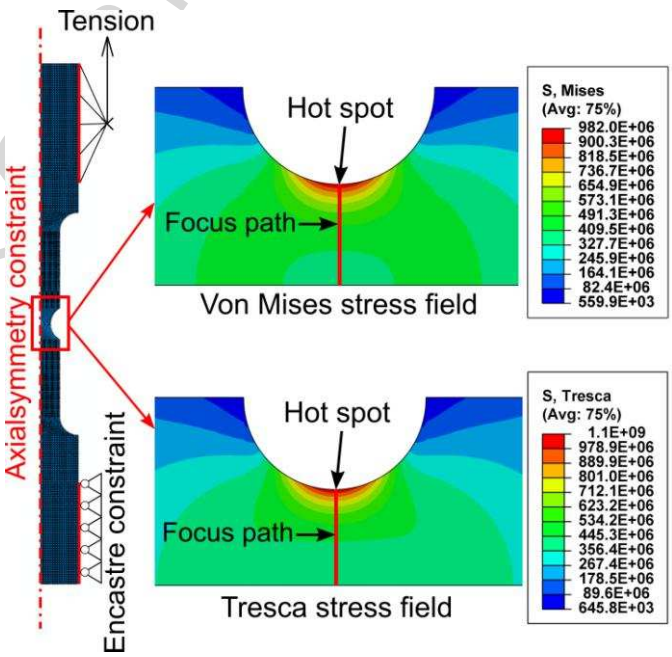

Figure 7. Von Mises and Tresca stress field located at the notch root of notched round bar specimen (notch radius=3.125 mm)

ACCEPTED MANUSCRIPT

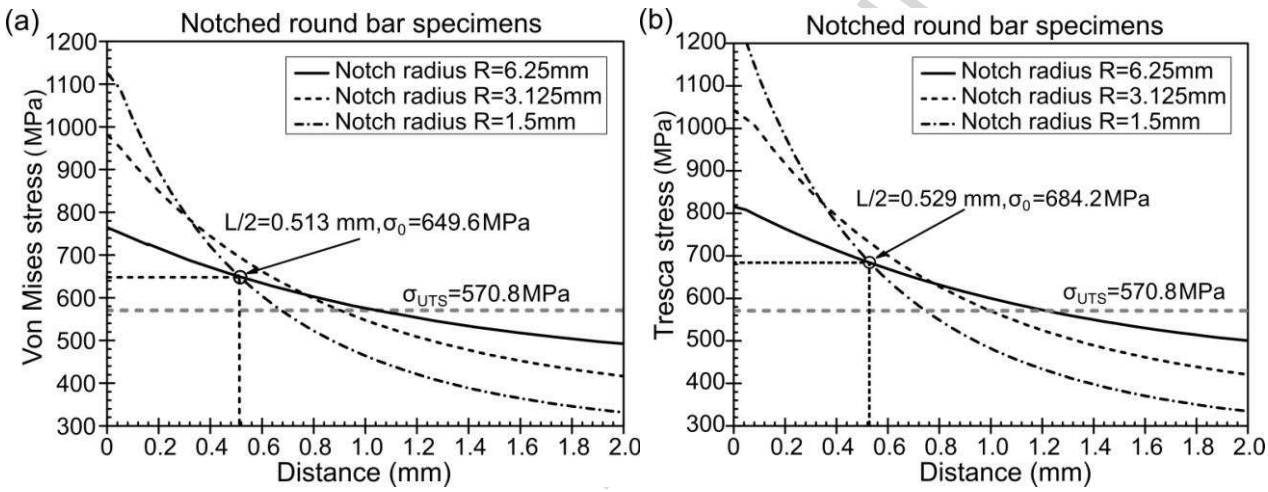

Figure 8. Stress-distance curves obtained on the corresponding focus paths of the notched round bar specimens: Von Mises stress (a); Tresca stress (b).

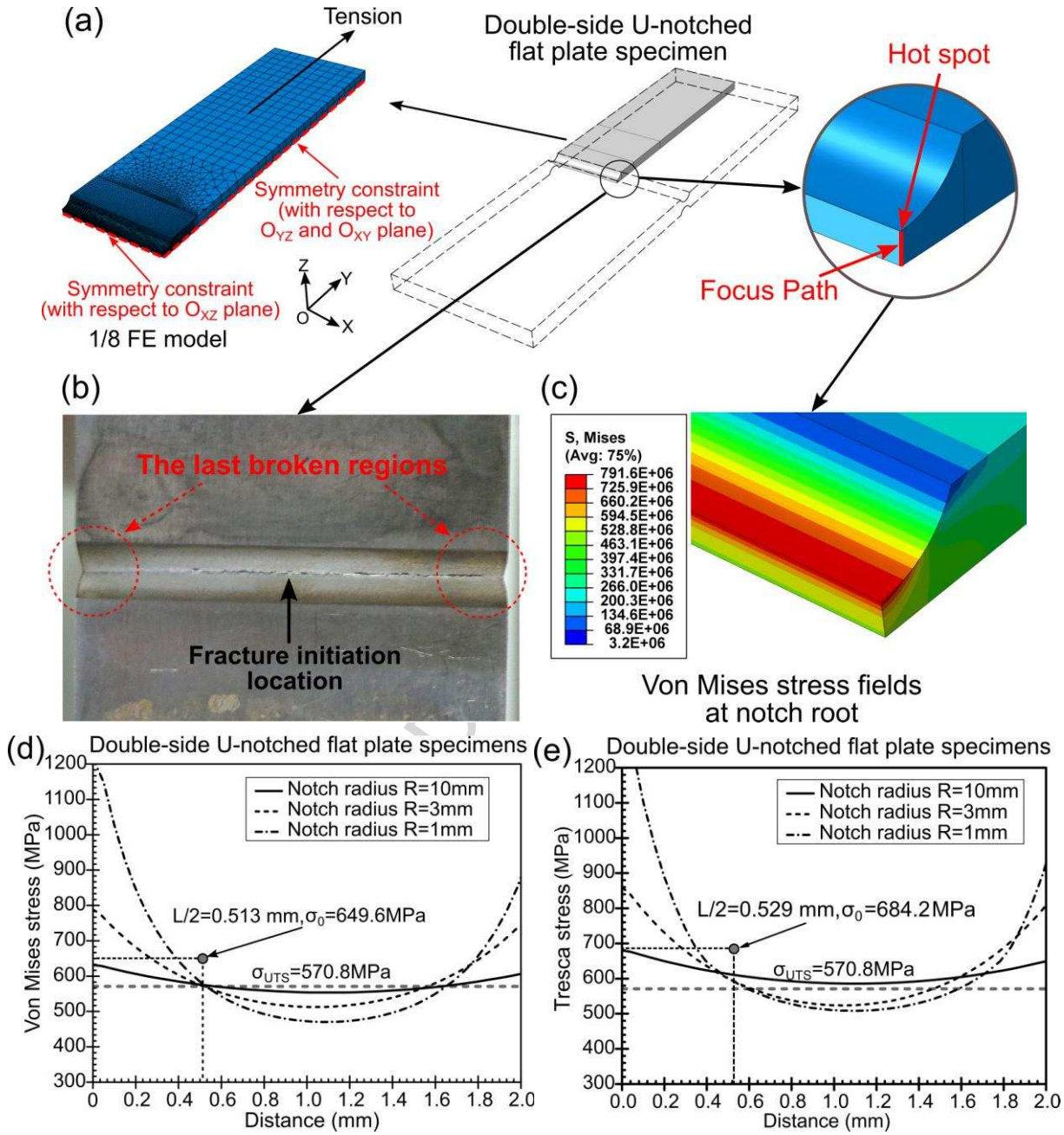

Figure 9. Finite element model and the focus path of double-side U-notched flat plate specimen (a); observed fracture initiation location of the sample in the test (b); Von Mises stress fields obtained at the notch root area (c); stress-distance curves obtained on the focus paths of the double-side U-notched flat plate specimens: Von Mises stress (d); Tresca stress (e).

ACCEPTED MANUSCRIPT

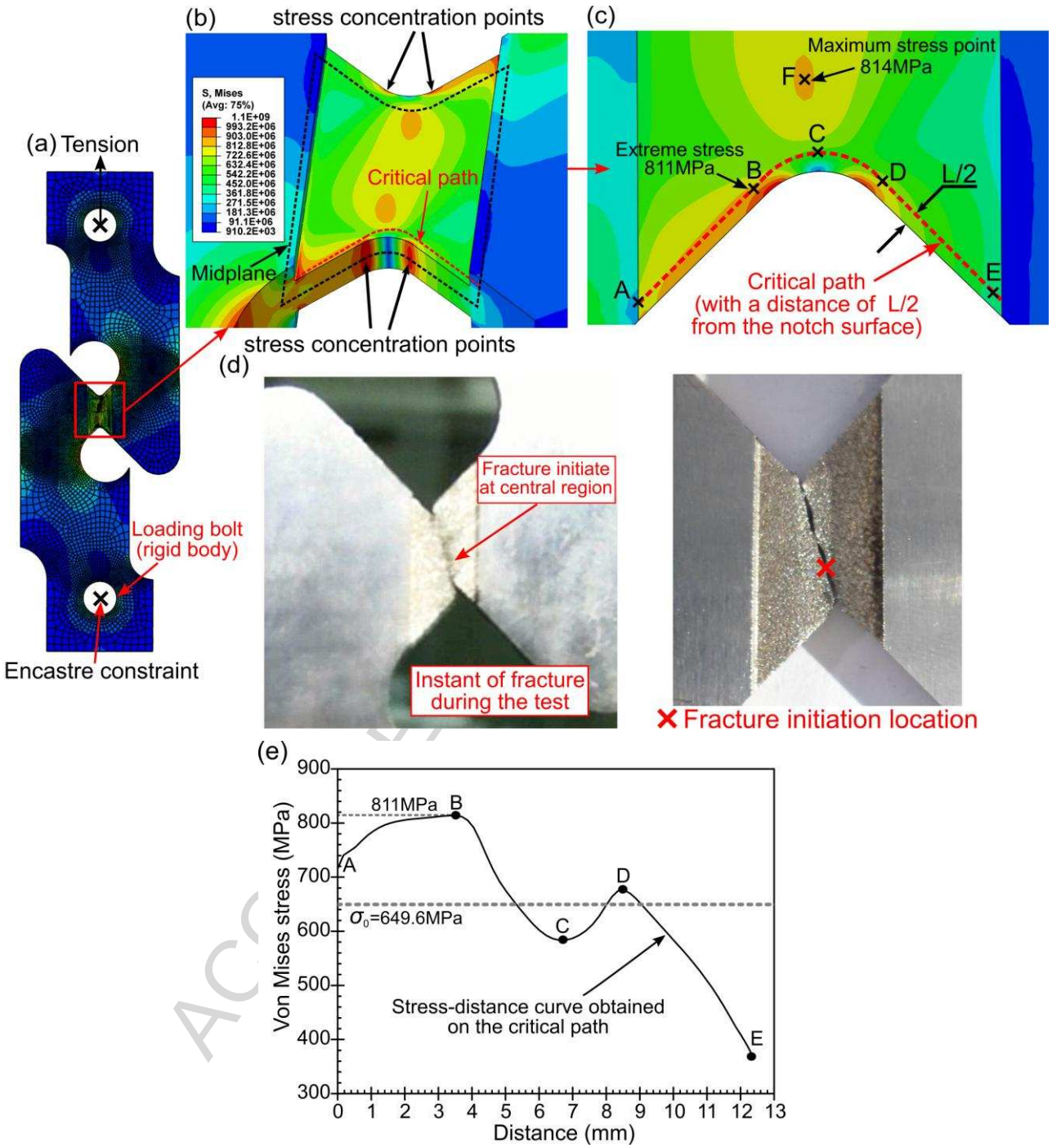

Figure 10. Finite element model developed for the pure-shear flat plate specimen (a); Von Mises stress fields located at the gauge section (b); the critical path located at the lower notch region of the specimen (c); the observed experimental fracture initiation location (d); Von Mises stress-distance curve obtained on the critical path (e).

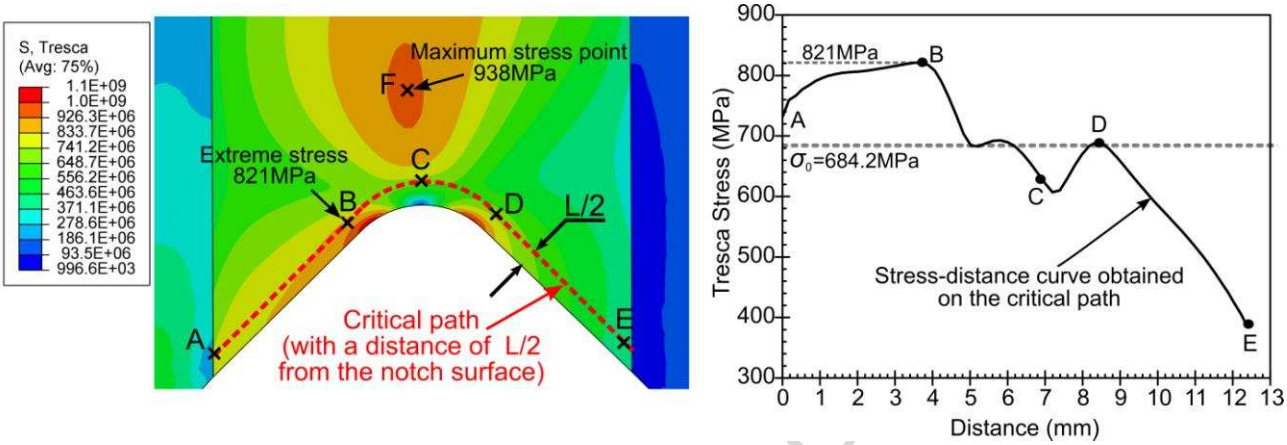

Figure 11. Tresca stress fields located at the gauge section of the pure-shear specimen and the relevant stress-distance curve obtained on the critical path

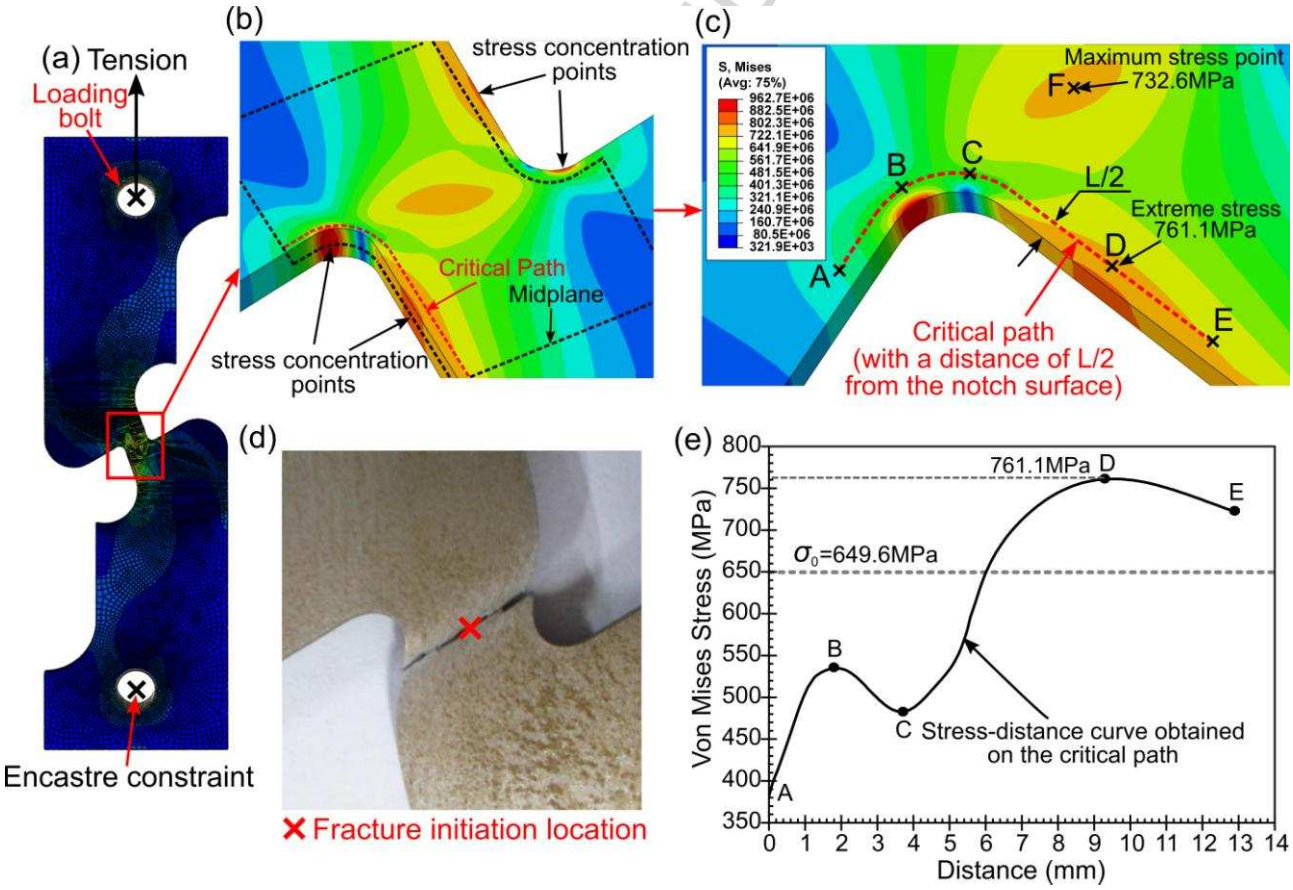

Figure 12. Finite element model developed for the tensile-shear flat plate specimen (a); Von Mises stress fields located at the gauge section (b); the critical path located at the notch region of the tensile-shear specimen (c); the observed experimental fracture initiation location (d); Von Mises stress-distance curve obtained on the critical path (e).

ACCEPTED MANUSCRIPT

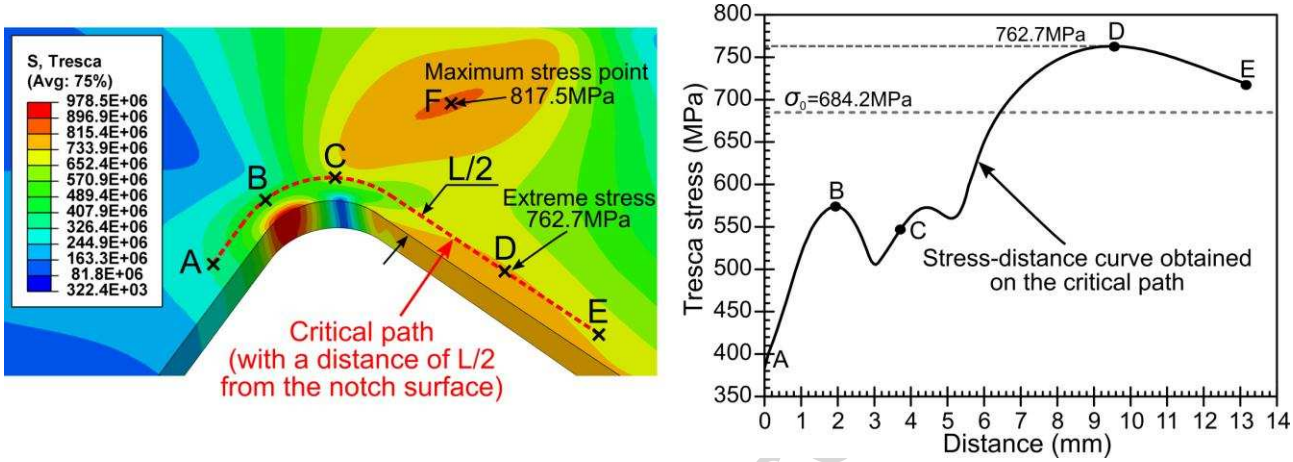

Figure 13. Tresca stress fields located at the gauge section of the tensile-shear specimen and the relevant stress-distance curve obtained on the critical path

ACCEPTED MANUSCRIPT

ACCEPTED MANUSCRIPT

Tables

Table 1 Chemical composition of Q460 steel (in weight%)

C	Si	Mn	P	S	Al	Nb	V	Ti
0.13	0.30	1.40	0.014	0.002	0.03	0.031	0.043	0.014

Table 2 Experimental results of the notched specimens tested in this paper

Specimen	Notch depth D(mm)	Notch opening angle (degree)	Notch radius R(mm)	Specimen code	Ultimate load F_u (kN)	Measured diameter (round bar specimen) or thickness (plate specimen)		Experimental loading rate (mm/min)
						Initial value (mm)	Value at fracture (mm)	
Notched round bar specimen	3.125	0	6.25	BN-1	21.68	6.32	3.76	0.3
				BN-2	21.54	6.38	4.68	
				BN-3	21.25	6.34	3.68	
			3.125	BN-4	23.89	6.38	4.62	0.2
				BN-5	23.59	6.38	4.12	
				BN-6	24.54	6.38	4.70	
			1.5	BN-7	25.67	6.60	4.28	
				BN-8	26.15	6.66	4.72	
				BN-9	25.56	6.66	4.52	
Double-side U-notched flat plate specimen	1.5	0	10	GP-1	68.14	2.16	0.94	0.24
				GP-2	66.69	2.24	1.06	
			3	GP-3	70.76	2.10	1.18	
				GP-4	71.37	2.06	1.00	
			1	GP-5	88.14	2.30	1.26	
				GP-6	93.56	2.06	1.36	
Pure shear flat plate specimen	3.97	90	2	FP-1	11.15	2.20	2.02	0.48
				FP-2	11.56	2.20	2.00	
Tensile shear flat plate specimen	——	80	3	FP-3	9.49	2.20	1.68	
				FP-4	9.57	2.20	0.94	

ACCEPTED MANUSCRIPT

Table 3 The accuracy of the PM and LM, used in conjunction with Von Mises stress, in predicting the static strength of notched round bar and double-notched flat plate specimens tested under uniaxial loading conditions

Specimen			Effective stress (Von Mises stress) σ_{eff} [MPa]		Estimate error [%]		Mean value of the error [%]	
Name	Notch radius	Specimen code	PM	LM	PM	LM	PM	LM
Notched round bar specimen	R=6.25mm	BN-1	672.5	609.5	3.53	-6.17	1.76	-7.74
		BN-2	656.0	594.5	0.99	-8.47		
		BN-3	654.5	593.8	0.76	-8.59		
	R=3.125mm	BN-4	692.7	590.2	6.64	-9.14	7.22	-8.63
		BN-5	684.2	582.8	5.34	-10.28		
		BN-6	712.5	607.4	9.69	-6.48		
	R=1.5mm	BN-7	649.0	538.7	-0.09	-17.07	-0.65	-17.55
		BN-8	649.0	538.4	-0.09	-17.11		
		BN-9	638.0	529.6	-1.78	-18.47		
Double side U-notched flat plate specimen	R=10mm	GP-1	591.1	594.1	-9.00	-8.54	-11.42	-11.18
		GP-2	559.6	559.8	-13.84	-13.82		
	R=3mm	GP-3	566.2	586.7	-12.82	-9.68	-11.84	-8.31
		GP-4	579.1	604.5	-10.85	-6.94		
	R=1mm	GP-5	536.7	559.8	-17.37	-13.82	-10.94	-2.31
		GP-6	620.2	709.3	-4.52	9.20		

Table 4 The accuracy of the PM and LM, used in conjunction with Tresca stress, in predicting the static strength of notched round bar and double-notched flat plate specimens tested under uniaxial loading conditions

Specimen			Effective stress (Tresca stress) σ_{eff} [MPa]		Estimate error [%]		Mean value of the error [%]	
Name	Notch radius	Specimen code	PM	LM	PM	LM	PM	LM
Notched round bar specimen	R=6.25mm	BN-1	694.4	624.4	1.50	-8.74	-0.04	-10.25
		BN-2	679.2	609.3	-0.72	-10.94		
		BN-3	678.1	608.3	-0.89	-11.08		
	R=3.125mm	BN-4	727.7	612.3	6.36	-10.50	6.93	-10.01
		BN-5	718.5	604.6	5.02	-11.63		
		BN-6	748.6	630.1	9.42	-7.91		
	R=1.5mm	BN-7	683.6	561.8	-0.08	-17.88	-0.70	-18.36
		BN-8	683.1	561.5	-0.16	-17.92		
		BN-9	671.5	552.3	-1.85	-19.27		
Double side U-notched flat plate specimen	R=10mm	GP-1	627.5	634.4	-8.27	-7.28	-10.74	-10.06
		GP-2	593.8	596.2	-13.21	-12.85		
	R=3mm	GP-3	586.4	620.0	-14.28	--	-13.35	--
		GP-4	599.2	636.5	-12.42	--		
	R=1mm	GP-5	551.7	597.3	-19.37	-12.70	-13.50	-12.70

ACCEPTED MANUSCRIPT

		GP-6	632.0	749.8	-7.63	--		

ACCEPTED MANUSCRIPT

ACCEPTED MANUSCRIPT

Highlights

- The static assessment of notched components made of Q460 steel is investigated
- Cracks of the samples containing complex notches initiate away from the stress raisers
- The TCD successfully estimates the strength of the samples with standard notches
- The TCD is able to evaluate the fracture behavior of the samples with complex notches

ACCEPTED MANUSCRIPT